



Modified Particle Swarm Optimization-Artificial Neural Network and Gene Expression Programming for Predicting High Temperature Oxidation Behavior of Ni-Cr-W-Mo Alloys

H. Hasibi^a, A. Mahmoudian^b, G. R. Khayati^{*a}

^a Department of Materials Science and Engineering, Shahid Bahonar University of Kerman, Kerman, Iran

^b Department of Metal, Institute of Science and High Technology and Environmental Sciences, Graduate University of Advanced Technology, Kerman, Iran

PAPER INFO

Paper history:

Received 24 May 2020
Received in revised form 28 July 2020
Accepted 02 August 2020

Keywords:

Artificial Neural Network
Gene Expression Programming
High-temperature Alloys
Modified Particle Swarm Optimization
Oxidation Behavior

ABSTRACT

This paper is an attempt to model the oxidation behavior of Ni-base alloys by considering the alloying elements, i.e., Cr, W, Mo, as variables. Modified particle swarm optimization-artificial neural network (MPSO-ANN) and gene expression programming (GEP) techniques were employed for modeling. Data set for construction of (MPSO-ANN) and GEP models selected from 66 cyclic oxidation performed in the temperature range of 400-1150 °C for 27 different Ni-based alloy samples at various amounts of Cr, W, and Mo. The weight percent of alloying elements selected as input variables and the changes of weight during the oxidation cycle considered as output. To analyze the performance of proposed models, various statistical indices, viz. root mean squared error (RMSE) and the correlation coefficient between two data sets (R^2) were utilized. The collected data of GEP randomly divided into 21 training sets and 6 testing sets. The results confirmed that the possibility of oxidation behavior modeling using GEP by $R^2 = 0.981$, $RMSE = 0.0822$. By consideration of oxidation resistance as criteria, Cr, Mo, and W enhanced the oxidation resistance of Ni-based alloys. The results showed that in the presence of Cr as alloying element, especially at Cr contents higher than 22 wt.%, the effect of W and Mo were negligible. However, the same trend was reversed at the sample with Cr content lower than 20 wt.%. In these cases, the effect of W and Mo on oxidation resistance were significantly enhanced.

doi: 10.5829/ije.2020.33.11b.23

1. INTRODUCTION

Ni-based alloys have extensive usages as high-temperature alloys due to relatively high resistance for the oxidation, e.g., structural materials for construction of the steam generator tubes and high-energy piping nozzles [1, 2]. Growing demand for new technologies enhanced the queries for advanced material with innovative properties, especially, high oxidation resistance, mechanical strength, and fabric ability. By consideration of these properties, alloys divided into the type with surface layer of Cr_2O_3 based scale for the oxidation behavior, and the type with Al_2O_3 -based scale

layer for protection against environmental agent [3–6]. Haynes alloy 230 is one of the most convenient Ni-based alloys with the surface layer of Cr_2O_3 based scale types. On the one hand, excellent high-temperature strength and on the other hand, acceptable environmental resistance has caused the evolution of Haynes 230 as a good candidate for application in high temperature components in aerospace as well as power industries [1]. According to literature, there would be endless queries for high-temperature structural alloys in the future, especially in power plants HR-120, HR-160 and Haynes 230 alloys are the most commercial chromium-forming alloys. The cycle oxidation

*Corresponding Author Email: khayatireza@gmail.com
(G. R. Khayati)

Please cite this article as: H. Hasibi, A. Mahmoudian, G. R. Khayati, Modified Particle Swarm Optimization-Artificial Neural Network and Gene Expression Programming for Predicting High Temperature Oxidation Behavior of Ni-Cr-W-Mo Alloys, International Journal of Engineering (IJE), IJE TRANSACTIONS B: Applications Vol. 33, No. 11, (November 2020) 2327-2338

resistance of these alloys is strongly dependent on the amount of alloying elements [7]. Specific characteristics of Haynes 230 alloys encourage the researchers to select as prime candidates for high-temperature usages. Accordingly, many studies have been designed for investigating the oxide scale formation as a function of operational temperature at different environmental conditions. For example, the presence of minor alloying elements in Haynes 230 significantly enhanced the oxidation resistance of alloys [4]. However, in some cases, some trend has been observed in binary alloys system at the presence of third alloying elements [4]. Investigating the literature revealed that the high-temperature resistance under thermal cycling condition of Cr_2O_3 -forming alloys is strongly affected by the amount of Si content [8]. Investigating the influence of Cr, W, and Mo on the oxidation resistance of Ni – Cr – W – Mo alloys is the main objective of this study. W and Mo constituents can enhance the high-temperature strength of high temperature alloys through solid solution hardening. While the oxidation resistance of Fe and Ni-base alloys are affected by W and Mo in various mechanisms. Typically, the presence of a higher contents of refractory metals, e.g., Mo, W, Ta, Re, is necessary for higher creep strength of Ni-based alloys [5, 9].

In their research, Yun et al. [1] proposed that accumulation of metallic Mo at the interface of oxide – metal and Mo^{6+} in Fe -24 wt.%, Cr -11 wt%. Mo-alloy has a high potential for the oxidation at 700 K and consequently enhanced the oxidation resistance. Similar observations have been reported about the positive effect of Cr and Al content in Ni-Co –Cr –Al –W –Mo – Ta –Re –Ru during the oxidation at 1100 °C and to the formation of a protective layer as NiAl_2O_4 [9]. In other researches, it has been shown that W and Mo cause volatile species as oxide phase to form and prevent the formation of fresh protective Cr_2O_3 layer after the spallation of oxide scale, and consequently there is not any linear relation between the amount of alloying elements and the oxidation behavior in the multi-component system [1]. Advances in computer hardware have made soft computing techniques more efficient. In addition, soft computing techniques may be used to model problems where the conventional approaches, such as regression analysis, fail or perform poorly [10]. Artificial neural networks, fuzzy logic, adaptive neuro-fuzzy interfaced, and GP are the most common soft computing techniques [11]. Use of AI techniques such as artificial neural networks (ANN) and gene expression programming (GEP) are popular in various fields of mathematics, engineering, medicine, economics, meteorology, and psychology are attracting interest in recent years [12]. ANN method provides a novel approach to predict the deformation behavior of materials under different conditions. ANN is an

artificial intelligence technology to simulate biological processes of the human brain [13, 14]. This system comprises operators interconnected via one-way signal flow channels. It collects the samples with a distributed coding which forms a trainable non-linear system. It is also self-adaptive to the environment to respond to the different inputs rationally [15]. Although ANNs typically build “black box” models, explicit formulas can be derived for a trained ANN model. A derivative-free optimization algorithm should be added to the training process of the ANN algorithm to avoid local minima, which leads to false convergence of the ANN model [10]. There are many papers on the applications of GEP in the literature for different engineering problems [11]. GEP is newer than the GP approach. GA by employment of genetic variation and operators selects the best individuals [12]. A combination of regression strategies and systematic design of the experiment is an efficient alternative approach for providing the experimental data in a new popularity model approach such as Gene expression programming. ANN and GEP can capture complex interactions among input/ output variables in a system without using prior knowledge about the nature of these interactions. To the best of our knowledge, there are some reports about the usage of two different AI applications: ANN and GEP together to compare prediction performance and explain experimental procedures [10, 11, 16–18].

This paper aims to evaluate the oxidation behavior of Ni-base alloys using PSO- ANN and GEP models [17]. In the current study, GEP (an advanced approach in artificial intelligent and modified PSO-artificial neural network strategy) has been utilized to construct a new model for the prediction and optimization of the oxidation resistance of Ni–Cr–W–Mo alloys as a function of main alloying element (i.e., Cr, W, Mo) using the reported data in the literature [1] as input. The samples produced by a combination of nominal composition in vacuum arc remelting furnace. XRD (X'pert MPD system of Philips instrument by Cu-K_α) and FESEM (MIRA3 model) were employed for phase analysis and morphological investigation, respectively. The motivation of this paper is to illustrate an appropriate model for the prediction of oxidation resistance of Ni–Cr–W–Mo alloys by artificial intelligence models as a function of the type and amount of alloying elements, (Cr, W, Mo) as well as determining the relative significance of input variable in output.

2. COLLECTION OF EXPERIMENTAL DATA

Determination of effective practical parameters as input has a key role in accurate modeling of specific output. Dae Won Yun et al. [1] have investigated the high-

temperature behavior of Ni–Cr–W–Mo alloys using Bayesian neural network. They used 66 experiments of oxidation cyclic on 27 samples of Ni–Cr–W–Mo alloys with various alloying elements. According to their experiments the oxidation cyclic behavior is mainly a function of alloying elements. Hence, various alloying content of Cr (18, 22, 26 wt.%), W (10, 14, 18 wt.%) and Mo (0, 2, 4 wt.%) were selected for the preparation of 27 different samples of Ni-base alloys. The alloying element content are selected as input and the weight changes after 66 cycles (mg/cm^2) are considered as output. Table 1 shows the chemical composition and corresponding weight changes for every sample [1].

TABLE 1. The details of experimental data for constructing of the GEP and modified PSO- ANN models [1]

Alloys name	Input			Output
	Cr (wt. %)	W (wt.%)	Mo (wt.%)	Weight changes after 66 cycles (mg/cm^2)
T01	18	10	0	-218.77
T02	18	10	2	-136.69
T03	18	10	4	-146.65
T04	18	14	0	-182.14
T05	18	14	2	-149.80
T06	18	14	4	-124.40
T07	18	18	0	-156.25
T08	18	18	2	-126.72
T09	18	18	4	-81.98
T10	22	10	0	-37.03
T11	22	10	2	-31.52
T12	22	10	4	-25.63
T13	22	14	0	-43.50
T14	22	14	2	-26.99
T15	22	14	4	-21.44
T16	22	18	0	-50.09
T17	22	18	2	-32.85
T18	22	18	4	-17.24
T19	26	10	0	-2.10
T20	26	10	2	-4.73
T21	26	10	4	-4.97
T22	26	14	0	-6.06
T23	26	14	2	-4.90
T24	26	14	4	-4.76
T25	26	18	0	-9.80
T26	26	18	2	-7.01
T27	26	18	4	-3.90

As shown in Figure 1(a), the effective formation of Ni-based alloying was confirmed in the typically XRD pattern of T13 sample. Minor segregation of W and Cr are the other events shown in Figure 1(b). the EDX point chemical analysis Figure 1(c) confirmed the presence of alloying elements in point A.

2. 1. Artificial Neural Network (ANN)

ANN is a biologically inspired system developed to solve problems in the same way that the human brain would. Generally, the architecture of ANN consists of three different layers as follows i.e., input layer, hidden layer and output layer [19–23]. Back propagation is one of the most common methods for training ANN. The weight vector of network is also important since it is contributing to the better performance [24–26]. The meta-heuristic techniques have been getting attention to improve the parameters of ANN. Therefore, we apply PSO algorithm to optimize ANN'S weights [14, 27].

2. 2. Particle Swarm Optimization (PSO)

Particle swarm optimization (PSO) is one of the most popular population-based stochastic optimization

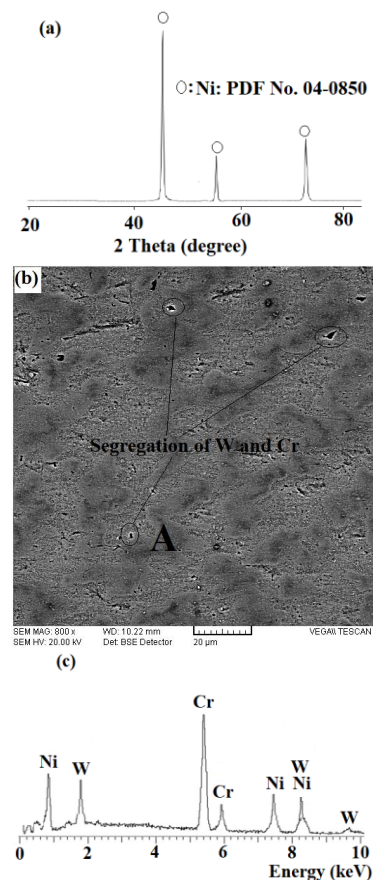


Figure 1. Typically illustration of (a) XRD pattern and (b) FESEM image and (c) EDX point chemical analysis of point A of as-cast T13 prepared alloy

algorithms [28]. PSO technique has received wide attention in recent years since it can converge to the optimization value quickly and has excellent robustness [29, 30]. The aim of the current study is to determine the most appropriate values for the weights and bias of NN (i.e., optimized NN) based on the PSO algorithm [31]. Then, we used optimized NN as the Fitness function of PSO to obtain the best values, of our futures.

2. 3. GEP Methodology

GEP is an advanced evolutionary approach with the ability to model the high complexity problems by the employment of a linear representation of a practical process with nonlinear behavior [32]. GEP provides a simple genetic operator, similar to the genetic algorithm, for the illustration of complex and expressive trees similar to the genetic programming [33, 34]. GEP, at first, dedicating a constant length of a chromosome to the initial population that is randomly generated [35]. At second step, the fitness of individuals of chromosomes is estimated and at the third step, by considering the higher fitness as criterion, the most appropriate individuals are selected to enhance the model accuracy. These stages are repeated until pre-defined generations number or until an appropriate model has been determined. Figure 2 illustrates the flowchart of Gene expression programming [36].

The input and output parameters for GEP modeling are the content of alloys elements, including Cr, Mo, W, and the weight changes after 66 cycles (mg/cm^2), respectively. To construct the GEP models, 21 set of experiments were employed for training and the remaining 6 sets were utilized for testing of the proposed models. GEP starts by random selection of 21 data set for training and 6 data set for testing the performance of proposed models. To model the oxidation behavior of Ni-base alloys, in the current study, GEP modeling was performed at the following steps:

1. Evaluation of the fitness of generated chromosomes by consideration of root relative squared error (RRSE) as fitness function;
2. Selection of the terminals and functions to construct the GEP chromosomes;
3. Determination of chromosomes architecture, i.e., a function of head size and gene number;
4. Definition of genetic operators and their related rates;
5. Finding of appropriate function for connecting the genes, i.e., “division”, “multiplication”, “subtraction”, and “addition” in GEP software [37].

Hence, GEP modeling is a time-consuming and complicated process [37]. By utilization of trial and error during the changing of GEP characteristics (as shown in Table 2) and monitoring the accuracy criteria until the acceptable models were obtained [38].

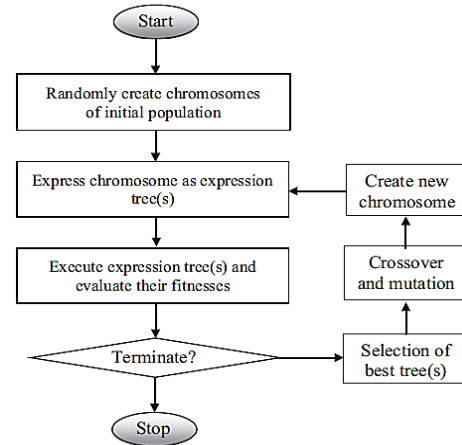


Figure 2. Providing the GEP flowchart [10]

TABLE 2. The characteristics of the training parameters of GEP models

GEP parameters definition	Choice
Function set	+, -, *, /, $\ln(x)$, x^2 , $\sqrt[3]{x}$, Tanh(x), Sech(x), Exp(x), atan(x), Max(x,y), Min(x,y), Not, Avg2, pow
Number of chromosomes	30
Head size	7,8 (GEP-10,GEP-11,GEP-12)
Number of genes	3
Linking function	Addition, multiplication
Fitness function error type	RRSE
Constant per gene	1
Mutation rate	0.00138, 0 (GEP-2, GEP-3, GEP-4, GEP-6, GEP-7, GEP-10, GEP-11)
Inversion rate	0(GEP-2, GEP-3, GEP-4, GEP-11), 0.00546 (GEP-1, GEP-5, GEP-8, GEP-9, GEP-12), 0.0082 (GEP-6, GEP-7, GEP-10)
One point recombination rate	0(GEP-2, GEP-3, GEP-4, GEP-11), 0.00277 (GEP-1, GEP-5, GEP-8, GEP-9, GEP-12), 0.0028 (GEP-6, GEP-7, GEP-10)
Two point recombination rate	0(GEP-2, GEP-3, GEP-4, GEP-11), 0.00277 (GEP-1, GEP-5, GEP-8, GEP-9, GEP-12), 0.0028 (GEP-6, GEP-7, GEP-10)

3. RESULTS AND DISCUSSIONS

Since GEP and MPSO-ANN are able to model specific output as a function of independent variables, the dependency of input variables must be checked at first. It was necessary to note that the presence of any dependency between input parameters, i.e., Cr (wt.%), W (wt.%), and Mo (wt.%) can evolve the problem and

exaggerate the strength of each input variable. This study used bivariate correlation analysis to determine the relationship between the practical parameters. Table 3 shows various correlation coefficients between practical parameters [39, 40]. As shown, there is not any interaction between the input parameters, and consequently, the collected experimental data set are appropriate for modeling by GEP and PSO-ANN.

3. 1. MPSO-ANN Model Results The evolution of 10 most appropriate MPSO-ANN models has been carried out by employment of two statistical indices, viz. root mean square error (RMSE) and the correlation coefficient between two data sets (R^2). It was necessary to note that the network with values of error indices closer to zero and value of R^2 closer to one shows better performance. Equations (1) and (2) show these indices.

$$RSME = \sqrt{\frac{1}{n} \sum_{i=1}^n (h_p - h_a)^2} \tag{1}$$

$$R^2 = 1 - \frac{\sum_{i=1}^n (h - h_p)^2}{\sum_{i=1}^n (h - h_a)^2} \tag{2}$$

in which, h_a , h_p , h_a^- and n are the experimental (target) value (actual weight changes after 66 cycles (mg/cm^2)), the predicted value of weight changes, the average of the actual value of weight changes during the two-run of measurements and the number of experimental samples, respectively.

Table 4 compares the 10 most appropriate MPSO-ANN models for the prediction of the oxidation resistance of Ni-based alloys in detail. As shown, various functions and neuron numbers caused the changes in the number of statistical indices. In addition, logsig and tansig are employed as activation functions during the optimization process.

Figure 3 compares the statistical indices for validation of proposed MPSO-ANN performances. In the case of RMSE (Figure 3(b)), the lower values of error belong to model 5 and consequently, this model shows higher performance with respect to the other. This situation belongs to model 9 for the case of R^2 as a threshold, because of its closer values to 1 (Figure 3(a)). If Fitness value, defined as the amount of both types of indices (error and R^2), the behavior of the proposed model as a function of network number can be monitored as shown in Figure 4. Accordingly, by

TABLE 4. Details of trained MPSO-ANN models

Model	Neurons	Function	R^2	RMSE
PSO-ANN 1	8-7-1	logsig-purelin	0.8532	0.0086
PSO-ANN 2	8-4-1	tansig-purelin	0.9118	0.0003
PSO-ANN 3	8-8-1	tansig-purelin	0.8636	0.0005
PSO-ANN 4	8-3-1	logsig-purelin	0.7795	0.0008
PSO-ANN 5	8-14-1	logsig-purelin	0.8635	0.0002
PSO-ANN 6	8-12-1	tansig-purelin	0.8141	0.0048
PSO-ANN 7	8-17-1	logsig-purelin	0.8607	0.0006
PSO-ANN 8	8-28-1	logsig-purelin	0.8607	0.0006
PSO-ANN 9	8-25-1	tansig-purelin	0.9337	0.0014
PSO-ANN 10	8-16-1	logsig-purelin	0.9006	0.0030

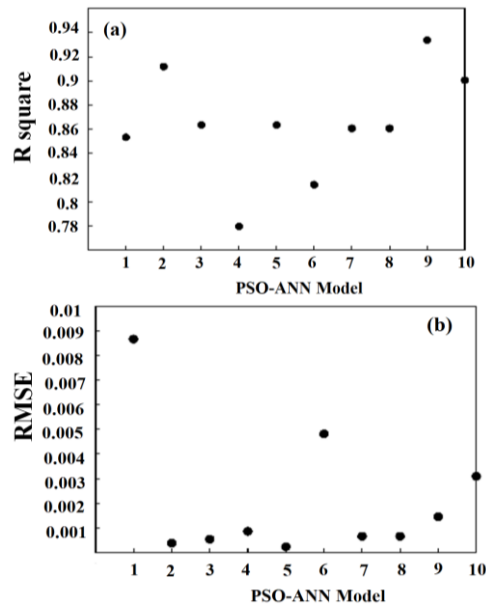


Figure 3. The statistical quality criteria of PSO-ANN networks (a) R^2 , (b) RMSE

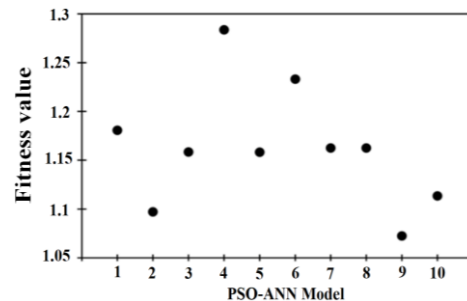


Figure 4. Fitness values of different ANN-PSO networks

TABLE 3. Dearson’s correlation coefficients among all pairs of input variables

Parameters	Cr (wt.%)	W (wt.%)	Mo (wt.%)
Cr (wt.%)	1	0	0
W (wt.%)	0	1	0
Mo (wt.%)	0	0	1

consideration of both types of indices, including R^2 and RMSE, model 9 proposed as the most appropriate models in this study. Because of the best performance

was achieved when fitness value was closer to zero. Fitness value was proposed as Equation (3):

$$\text{Fitness value} = \text{RMSE} - \frac{1}{R^2} \quad (3)$$

In Figure 5, normalized data of weight loss as a function of various alloying elements have been reported and confirmed the acceptable performance of MPSO-ANN network. In addition, the accuracy of MPSO-ANN 9 network is higher for the estimation of the effect of Cr, W, and Mo.

3. 2. GEP Model Results

In current work, GEP, i.e., an advanced methodology in AI has been utilized to model the oxidation behavior of Ni-based alloys in the presence of Cr, W, and Mo as alloying elements. Hence, 12 different GEP models were proposed after evaluation of 100 models constructed with various GEP parameters including chromosome number, head size, gene number, linking function and function set [12].

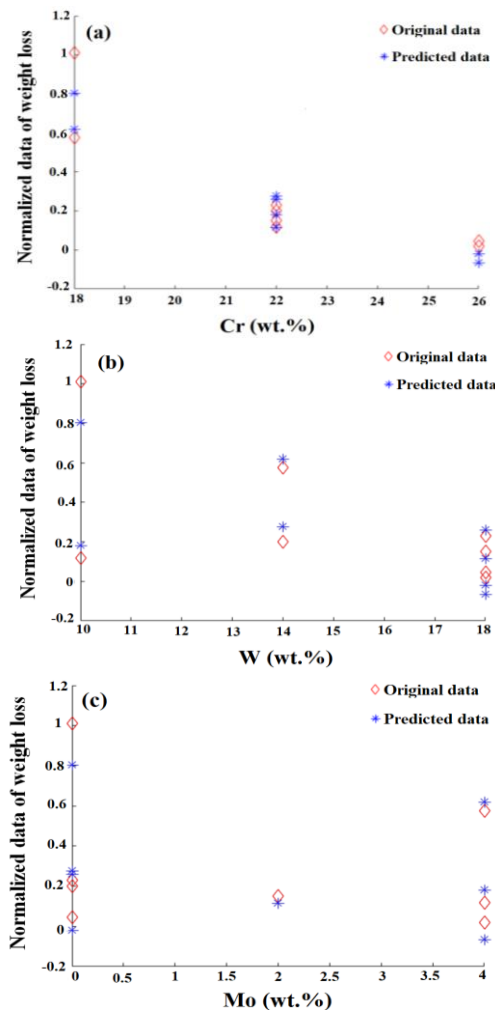


Figure 5. Predicted weight loss based on alloying elements Cr(a), W(b) and Mo(c) by hybrid ANN and MPSO algorithm

It was necessary to note that due to the possibility of various combination in GEP parameters, construction of GEP model for all these combinations need a huge amount of computational time. Table 5 indicates the training and test evaluation of GEP model after 66 oxidation cycles. In a similar approach for validation of PSO-ANN networks, the statistical indicator including root mean square error (RMSE) and an absolute fraction of variance (R^2) are utilized for validation of the accuracy GEP models [41]. As shown in Table 4, R^2 values changed in the range of 0.938-0.991 for the training step and 0.931-981 for the testing step. The minimum amount of RMSE is equal to 0.0572 in testing and 0.0279 for the training step, respectively. By consideration of the higher value of R^2 (close to 1) and lower value of RMSE (close to zero) as criteria, GEP-12, GEP-11, GEP-8 and GEP-9 were selected from 100 GEP investigated models. Figure 5 compares the changes of statistical indicators in training and testing of most appropriate GEP models. Analysis of Figure 6 reveals that GEP-11 shows higher accuracy with respect to the other GEP models in prediction of high-temperature oxidation behavior of Ni-Cr-W-Mo alloys.

Table 6 Summary of the most appropriate 12 GEP models.

Figure 7 shows the comparison of R^2 and MSE for GEP-8, GEP-9, GEP-11 and GEP-12 models in testing and training phases. In these Figures, the sample numbers shown in circles and hexagons, while the numbers in vertical axis belong to the weight changes after 66 cyclic oxidation tests. As can be seen, R^2 and RMSE training and testing of GEP-11 model confirmed the higher accuracy of GEP-11 respect to the other

TABLE 5. Statistics indicator values for the validation of proposed GEP models

Model	R^2		RMSE		Best Fitness	
	Train	Test	Train	Test	Train	Test
GEP-1	0.9380	0.9382	0.0770	0.0713	799.5	795.20
GEP-2	0.9706	0.9465	0.0529	0.0977	853.03	739.19
GEP-3	0.9903	0.9662	0.0302	0.0875	910.46	759.77
GEP-4	0.9445	0.9759	0.0731	0.0914	804.81	751.84
GEP-5	0.9913	0.9553	0.0290	0.1019	913.55	730.96
GEP-6	0.9738	0.9485	0.0528	0.0979	835.6	738.78
GEP-7	0.9867	0.9314	0.0354	0.0782	896.52	779.84
GEP-8	0.9824	0.9700	0.0412	0.0596	881.75	882.87
GEP-9	0.9887	0.9715	0.0325	0.0572	904.15	828.74
GEP-10	0.9823	0.9559	0.0408	0.0686	882.74	801.48
GEP-11	0.9919	0.9812	0.0279	0.0822	771.01	916.53
GEP-12	0.9637	0.9774	0.0604	0.063	835.62	813.66

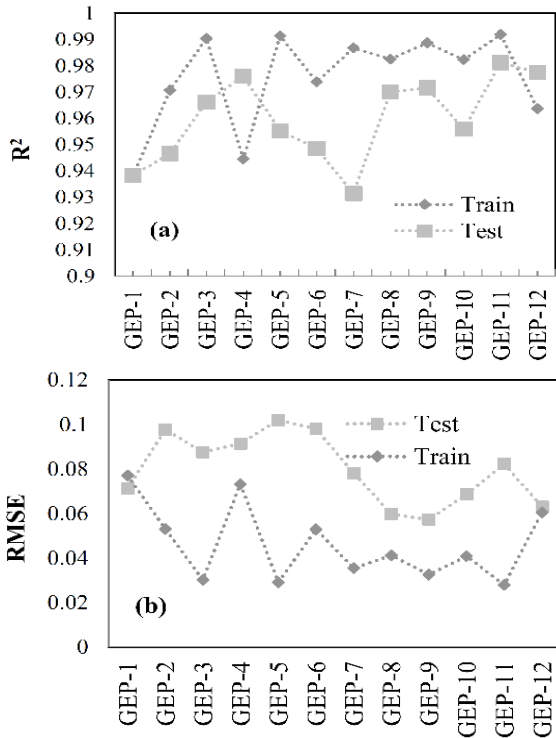


Figure 6. Different errors for training and testing data series in GEP models; (a) R² and (b) RMSE

models (Figures 7 (e) and 7 (f)). Accordingly, the empirical weight changes, after 66 cycles of oxidation of Ni-Cr-W-Mo alloys are in good agreement with the predicted weight variation with GEP-11.

Boxplot is a popular approach for the visual representation of data sets through their quartiles. Whisker, i.e., parallel lines extending from the boxes, is utilized to show the variability region at the upper and lower quartiles. Outliers are often shown as separate dots in the line with whiskers. Taking less space as well as its ability for comparing the distribution of any data set is the main advantage of boxplot [42]. Boxplot provides the possibility of determination of the outliers the symmetricity of data, the amount of data set tightly, direction, and amount of skewed diagrams as a visual representation.

To find the best model for the explanation of the oxidation behavior of Ni-Cr-W-Mo alloys, boxplot is utilized in this study. Accordingly, the residual error, defined as the difference between the predicted and experimental values, is plotted for various GEP models. Figure 8 compares the boxplot of the training and testing phase for various GEP models [42].

In boxplot, the rectangle displays the distance between the first and third quarters and the line within the rectangle determines the second quarter. The black lines outside the rectangle show the minimum and

maximum data values. Moreover, the outliers are illustrated in boxplot. As shown in Figure 8, GEP-11 and GEP-8 have shown the lowest amount of residual error. However, GEP-8 model illustrates higher outliers and caused a severe reduction of its performance. Moreover, exception the GEP-8 and GEP-12, the data tend toward the higher values and their distribution skewed to the top [42]. In Figure 8 b, all GEP models show at least one outlier data exceptional the GEP-12 with to outliers. In addition, GEP-8 and GEP-11 have lower values of residual errors.

TABLE 6. Summary of most appropriate GEP models in the prediction of the oxidation resistance

Model	Infering equation
GEP-1	$y = \min(\text{GEP3Rt}((\text{Cr} * \text{Mo}) + \text{GEP3Rt}((\text{W} + 0.492))), \text{Mo}) + ((1.0 - \text{Cr}) * (-0.640)) * (1.0 - \text{Cr}) * ((\text{Cr} + 0.640) ^ 2) + (((1.0 - \text{Mo}) - (-5.298 + \text{Mo})) + ((-5.298 + \text{Cr}) + \max(\text{Cr}, \text{Mo})) / 2.0) / 2.0$
GEP-2	$y = (((1.0 - \text{Mo}) - (-7.388 + \text{Mo})) + \max(((\text{Cr} + \text{Cr}) / 2.0), (\text{Mo} + \text{W}) / 2.0)) / 2.0 + (((1.0 - \text{Cr}) * (-0.659)) * (1.0 + 0.659)) * ((\text{Cr} - 0.659) ^ 2) + \min((((1.35) - (\text{Cr} - 0.675)) + \text{GEP3Rt}(0.675)) / 2.0), \text{Mo})$
GEP-3	$y = ((\min(((\text{Cr} + \text{Cr}) + ((\text{W} + \text{Mo}) / 2.0)), \max(0.931, \text{Mo})) + \text{Cr}) / 2.0 + (1.0 / ((1.196 * (((\text{Cr} + \text{Cr}) + 1.196) + \exp(1.196)))) + (((0.281 * \text{W}) * \text{Mo}) ^ 2) + ((\text{Cr} - 0.281) - (\text{Cr} ^ 2)) / 2.0)$
GEP-4	$y = \min((((((\text{Cr} + \text{Mo}) / 2.0) ^ 2) + \tanh((0.142 - \text{Mo})) / 2.0), \text{Mo}) + (((\min((\text{Cr} - 0.216), (\text{Mo} * 0.216)) + (\text{W} * 0.216)) / 2.0) + 0.216) + (\min((\text{Cr} + \text{Mo}), 0.759) + ((\text{Mo} * 0.759) - ((\text{Mo} + \text{Mo}) / 2.0)))$
GEP-5	$y = \tanh(((\text{GEP3Rt}(((1.940 + 2.486) / 2.0) + (\text{Cr} * \text{W})) ^ 2) ^ 2)) * \text{GEP3Rt}(\tanh((((((\text{W} + \text{Mo}) / 2.0) ^ 2) ^ 2) + \text{Cr})) * (((1.0 - \text{Mo}) + (\text{Cr} + \text{Mo}) - ((\text{Cr} ^ 2) + ((\text{W} + \text{Cr}) / 2.0)) / 2.0))$
GEP-6	$y = (((9.143 + (\text{Cr} + 9.143)) / 2.0) * ((9.143 - \text{Mo}) - (\text{Cr} ^ 2))) + ((\min(\text{Cr}, 0.139) - 0.278) + ((\text{W} * 0.139) * (\text{Cr} ^ 2))) + (((\text{Cr} + \text{W}) + (\text{Cr} + \text{Mo})) + ((1.0 - \text{W}) * (\text{Cr} + 0.45)) / 2.0)$
GEP-7	$y = \text{atan}(\exp(-0.707) * \text{GEP3Rt}(((\text{Cr} + \text{Mo}) / 2.0))) + \text{atan}(\text{atan}(\text{atan}(\text{GEP3Rt}(\max(\text{W} * 1.495, \text{Cr})))) + ((\text{GEP3Rt}(\text{Mo}) - \tanh(\text{Mo})) * (\max(0.804) - (1.0 - 0.402)))$
GEP-8	$y = ((\text{sech}(\text{Cr}) * (\text{Cr} + \text{Cr})) - \max(\max(0.113, \text{Cr}), (0.113 * \text{Cr}))) + (\text{atan}(\max(\text{Cr}, \text{W}) - (-0.612))) * ((0.374) - (\text{Mo} * \text{Cr})) + ((\min(\text{Mo}, \text{Cr}) + 0.321)) * \max((\text{Cr} * \text{Cr}), \text{atan}(\text{Mo}))$
GEP-9	$y = \text{atan}(\text{atan}((-0.757 * \text{Cr})) + ((\tanh(\text{Cr}) + \text{atan}(\text{Cr})) / 2.0)) + \text{atan}(\text{atan}(((\text{atan}(\text{Mo}) + ((0.110 + \text{W}) / 2.0)) / 2.0) + (\text{Cr} + \text{Cr}))) + \max((((0.418 + \text{Cr}) - \text{W}) * (1.0 - \text{Cr})), \text{atan}(0))$
GEP-10	$y = \text{GEP3Rt}(\tanh((((0.840 - \text{Mo}) - \exp(\text{Cr})) * \exp(\exp(\text{Cr})))) * ((\tanh((\max(\text{W}, \text{Cr}) + (\text{Mo} + \text{Cr})) + \text{GEP3Rt}(\text{Cr}) / 2.0) * \min((-1.004), \text{GEP3Rt}(((\text{Cr} - 0.502) - \tanh(\text{Mo}))))$
GEP-11	$y = \max((1.0 - (1.0 - \tanh(\text{Cr}))), ((\min(\text{W}, \text{W}) + (0.127 * \text{Mo})) / 2.0) ^ 2) + (((\text{GEP3Rt}(\text{GEP3Rt}(\text{Cr})) + (\text{Mo} * 0.237)) / 2.0) / ((0.474) + (\text{Cr} + \text{Cr}))) + ((((-0.347 * \text{Cr}) - (-0.347)) + \tanh((\text{Cr} ^ 2)) / 2.0) * (-0.347))$
GEP-12	$y = (((((1.0 - \text{Cr}) - \text{Mo}) + (-0.427 * \text{W})) / 2.0) * (((\text{W} + \text{Cr}) / 2.0) + (\text{Cr} - 0.427)) / 2.0) + (\tanh(\text{Cr}) - \min(\text{Cr} - (\text{Cr} + \text{W}), (-0.869))) + ((1.0 / (\text{reallog}(((0.472) / 2.0)))) + ((\tanh(\text{Cr}) - \text{Cr}) + ((\text{Mo} + \text{Cr}) / 2.0)) / 2.0)$

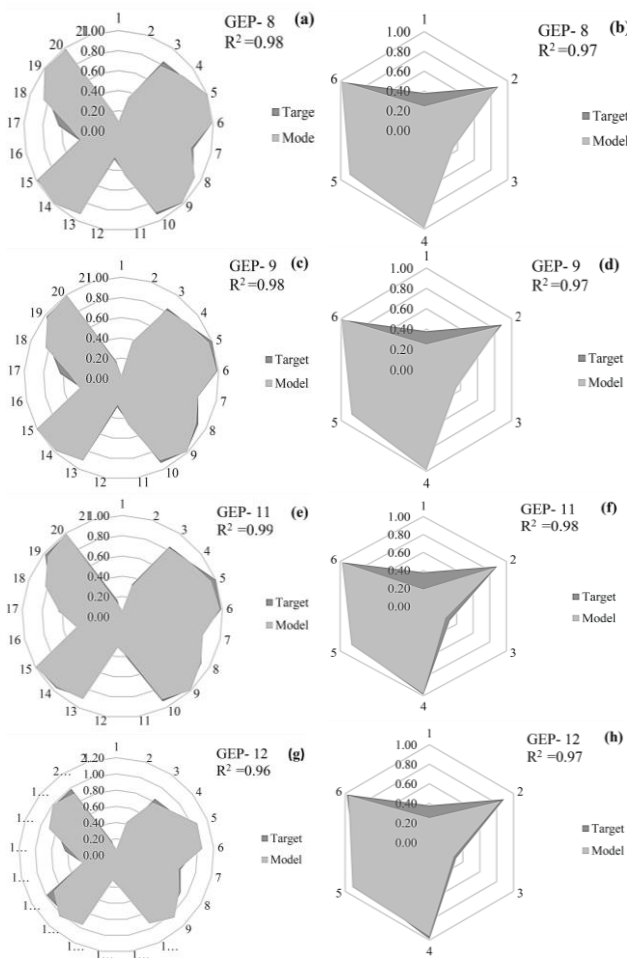


Figure 7. Comparison of R^2 and MSE for testing and training phases of the most appropriate model prepared by GEP; (a, b): training and testing of GEP-8; (c, d): training and testing of GEP-9; (e, f): training and testing of GEP-11; (g, h): training and testing related to GEP-12

Since, the aim of this study is to illustrate a model with the highest performances, the boxplot of 27 samples has been prepared by the most appropriate GEP models (Figure 9). Accordingly, in spite of the presence of an outlier in GEP-12, due to the wide distribution of residual error, this model was rejected. The other GEP models (GEP-8 and GEP-9) showed at least two outlier data, while GEP-11 has symmetrical distribution as well as one outlier data. Accordingly, GEP-11 has been proposed as the most appropriate model for prediction of the oxidation behavior of Ni-Cr-Mo-W alloys at high temperatures.

3. 3. Sensitivity Analysis Since, the proposed PSO- ANN network and GEP model have acceptable performance for the prediction of oxidation behavior, the sensitivity analysis was performed on both of them and the results were compared.

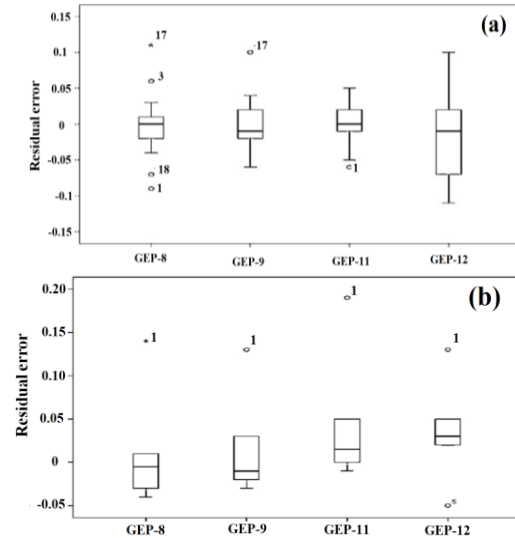


Figure 8. The values of residual error for GEP models in the form of boxplots for the (a) training and (b) testing datasets

3. 3. 1. Sensitivity Analysis using PSO- ANN Network

In this approach, the sensitivity analysis was performed by changing the values of each parameter in the range of lower and higher levels of practical values when the other parameters remained constant in their average values. In addition, to provide the possibility of illustration of all affected parameters with various values and their distribution, all inputs were standardized by definition of z- square [35].

$$Z = \frac{(h_i - \bar{h})}{\sigma} \tag{4}$$

where, h_i , \bar{h} , σ and Z are the i_{th} variable, the average, standard deviation of input parameters, and the standardized value of parameter, respectively. The display of weight changes versus the changes of any input parameters are shown in Figure 10. As shown, the change in the input parameter (Mo) versus the output parameter (weight changes after 66 cycles) is very small and it is as a straight line. Therefore, the weight percent of Mo has the least effect on the weight changes (oxidation resistance) while Cr and W have the most effect on oxidation resistance, respectively.

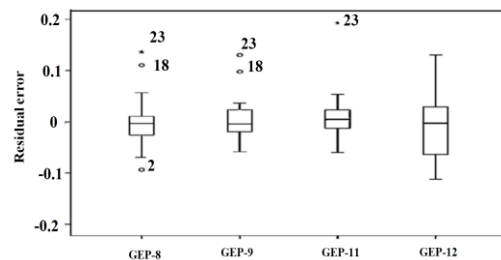


Figure 9. The values of residual error for GEP models in the form of box plots for all of 27 Ni-Cr-W-Mo alloys

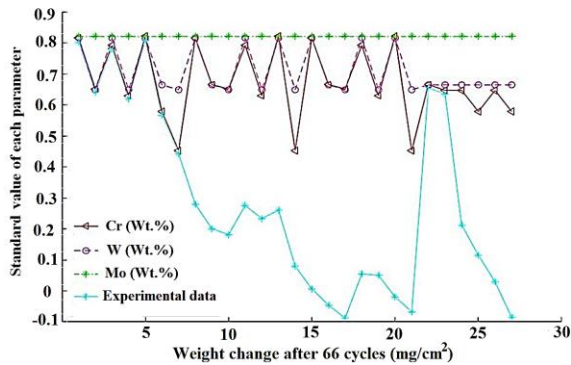


Figure 10. Sensitivity analysis of input parameters on the weight changes after 66 cycles [35]

3. 3. 2. Sensitivity Analysis using GEP Similar approach was used to determine the sensitivity analysis in current study. In this regard, various noises were created on the input data at 5 and 10 % and compared the amount of output error by actual values.

Figure 11 shows the sensitivity analysis to determine the relative significance of Cr content on the oxidation resistance of Ni-Cr-W-Mo alloys investigated in this study. According to this figure, the oxidation resistance of Ni-based alloys is proportional to their Cr content. Also, the positive effect of Cr amount on the oxidation resistance is more severe at higher Cr content, i.e., (T19-T27) alloys with 26 wt.% of Cr. However, the positive effect of Cr content in other samples with 22 and 18 wt.% of Cr is lower proportional to the amount

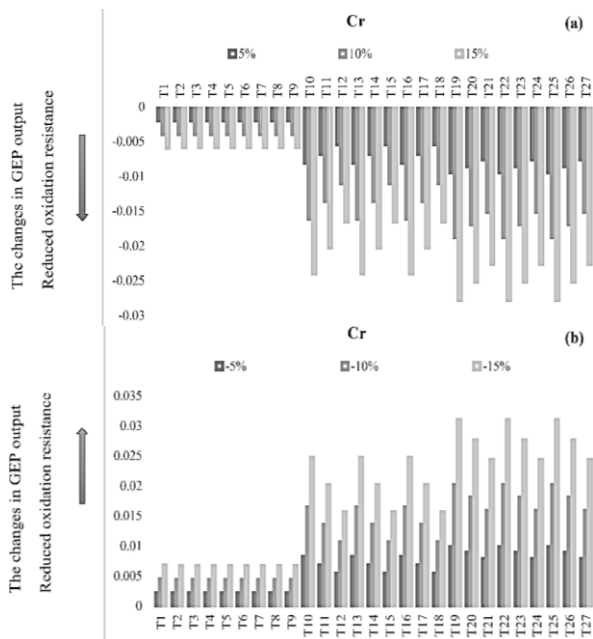


Figure 11. Sensitivity analysis for determination of the effect of Cr on the oxidation resistance of Ni-Cr-W-Mo alloys. (a) Increasing the Cr content, (b) Decreasing Cr content

of Cr in (T1, T2, T3, T4, T5, T6, T7, T8, T9), (T10, T11, T12, T13, T14, T15, T16, T17, T18) alloys. Moreover, the presence of Mo and W in the alloys with 22 wt.% and 26 wt.% of Cr decreased the positive effect of Cr in oxidation resistance. In this trend, W shows lower effect compared to Mo.

Figure 11 (b) reveals that the effect of reducing the Cr content on decreasing the oxidation resistance is higher in the sample with 26 wt.% of Cr with respect to the other. Also, the presence of Mo and W in alloys with 18 wt.% Cr compensates for the negative effect of lower Cr on the cyclic oxidation behavior. In this regard, Mo is more effective than the W.

The results of the sensitivity analysis on the effect of W content is shown in Figure 12. As shown in Figure 12 (a), similar to the effect of Cr, generally the addition of W amount enhances the oxidation resistance and this positive effect of W is more serious in alloys with the lower content of Cr. Also, by decreasing W content (Figure 12 (b)), oxidation resistance of low Cr content (18 wt.%) is decreased and this trend is intensified in the presence of Mo.

Analysis of Figure 13 (b) shows that similar trends to Cr and W have evolved in the presence of Mo on the oxidation resistance of Ni-Cr-Mo-W alloys. This effect is higher in low Cr content (18 wt.%) alloys. Moreover, decreasing Mo content decreased the oxidation resistance and this trend is more intensified in low Cr content alloys.

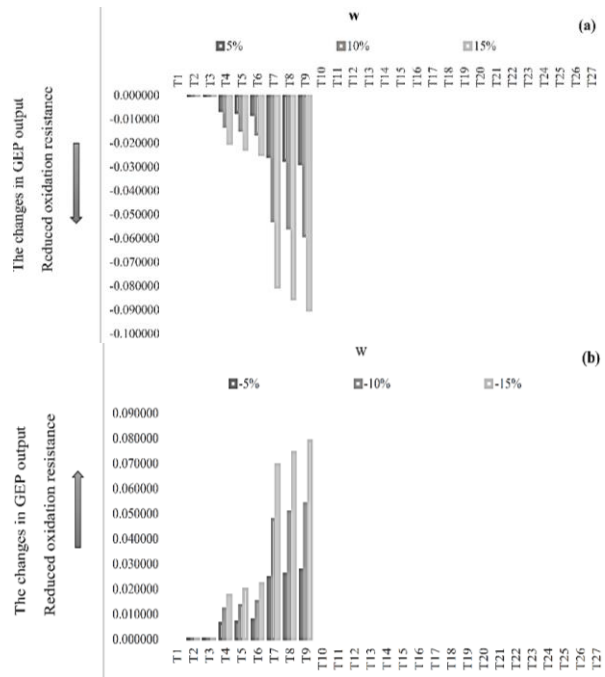


Figure 12. Sensitivity analysis for determination of the effect of W on the oxidation resistance of Ni-Cr-W-Mo alloys. (a) Increasing the W content, (b) Decreasing W content

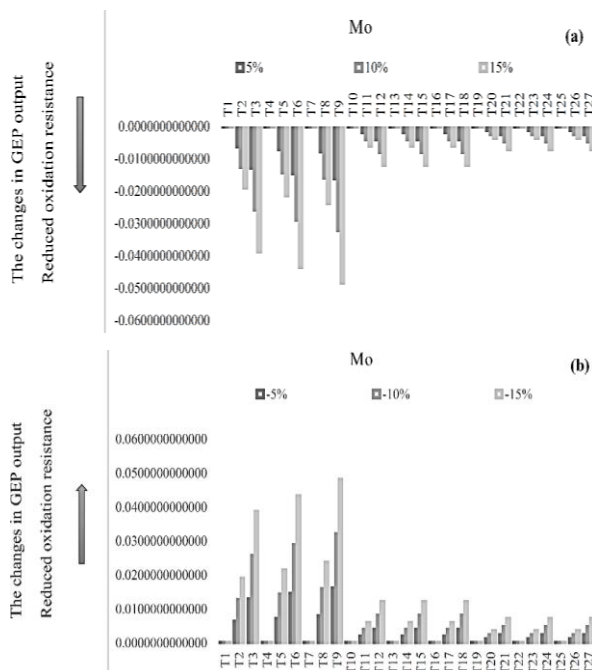


Figure 13. Sensitivity analysis for determination the effect of Mo on the oxidation resistance of Ni-Cr-W-Mo alloys. (a) Increasing the Mo content, (b) Decreasing Mo content

In conclusion, Cr, Mo and W enhanced the oxidation resistance of Ni-Cr-Mo-W alloys. However, in higher Cr containing alloys (alloys with 22 and 26 wt.% of Cr), the Cr content is administrated parameters on the oxidation behavior. The presence of Mo and W induced a positive effect on the oxidation behavior of 18 wt.% Cr. While this effect is reversed in high Cr content alloys (26 and 22 wt.% Cr).

In summary, the higher Cr contents facilitate the formation of adhesive Cr-rich oxide protective layer and induce higher temperature resistance. Typically in the alloys containing 26 wt.% Cr, the continuity and adhesivity of surface Cr_2O_3 layer disturbed in the presence of other alloying elements including W and Mo. It seems that these elements disturb the protective Cr_2O_3 surface films through the evaporation of W and Mo oxides [43]. While, in the case of alloys with Cr content lower than 22 wt.%, the effect of W and Mo were reversed. In this condition, such alloying oxides can provide robust surface protectivity of the oxide layer at high temperatures [44].

In Figure 14, the weight changes from experimental studies are compared with the predicted values using GEP- 11 and the MPSO-ANN 9 models. As can be seen, the values predicted by GEP- 11 model are more accurate than the MPSO model and are closer to real values and this means that the presented GEP model has achieved success in simulation of the high-temperature oxidation behavior of the Ni-based alloys.

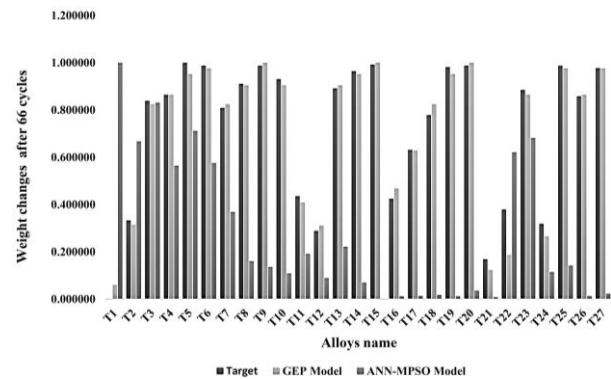


Figure 14. The comparison between the experimental weight changes (after 66 cycles) and the predicted weight changes by GEP and MPSO-ANN models

4. CONCLUSIONS

The prediction resistance of Ni-Cr-Mo-W alloys has a key role in the improvement and design of new high-temperature resistance materials. MPSO-ANN and GEP are increasingly being seen as a novel evolutionary algorithm, which enhanced many advantages of previously constructed models. Based on the results of the current study in which MPSO- ANN and GEP are utilized to model the oxidation behaviors of Ni-Cr-Mo-W alloys, confirmed that the GEP models have the higher performance for modeling of high-temperature resistance behavior. Accordingly, the GEP model and MPSO-ANN model with R^2 and RMSE values equal to 0.9919, 0.0279, 0.9337, and 0.0014, respectively proposed as appropriate models for prediction of the oxidation behavior of Ni-Cr-Mo-W alloys. Moreover, the sensitivity analysis revealed that at higher Cr content (i.e., 22 and 26 wt.%), Cr was administrated alloying elements on the high-temperature resistance, while, in the lower Cr content (i.e., 18 wt.%), the presence of Mo (with the higher effect), and W (with the lower effect) can compensate the lower content of Cr content.

5. REFERENCES

1. Yun, D. W., Seo, S. M., Jeong, H. W., Kim, I. S., and Yoo, Y. S. "Modelling high temperature oxidation behaviour of Ni-Cr-W-Mo alloys with Bayesian neural network." *Journal of Alloys and Compounds*, Vol. 587, (2014), 105–112. <https://doi.org/10.1016/j.jallcom.2013.10.138>
2. Smola, G., Gawel, R., Kyzioł, K., Miszczak, M., and Grzesik, Z. "Influence of Nickel on the Oxidation Resistance at High Temperatures of Thin Chromium Coatings." *Oxidation of Metals*, Vol. 91, No. 5–6, (2019), 625–640. <https://doi.org/10.1007/s11085-019-09899-w>
3. Cho, S. H., Lee, S. K., Kim, D. Y., Lee, J. H., and Hur, J. M. "Effects of alloying elements of nickel-based alloys on the hot-corrosion behavior in an electrolytic reduction process." *Journal of Alloys and Compounds*, Vol. 695, (2017), 2878–2885.

- <https://doi.org/10.1016/j.jallcom.2016.11.394>
4. Tawancy, H. M. "On the behaviour of minor active elements during oxidation of selected Ni-base high-temperature alloys." *Materials at High Temperatures*, Vol. 34, No. 1, (2017), 22–32. <https://doi.org/10.1080/09603409.2016.1231861>
 5. Olivares, R. I., Young, D. J., Nguyen, T. D., and Marvig, P. "Resistance of High-Nickel, Heat-Resisting Alloys to Air and to Supercritical CO₂ at High Temperatures." *Oxidation of Metals*, Vol. 90, No. 1–2, (2018), 1–25. <https://doi.org/10.1007/s11085-017-9820-7>
 6. Kim, H. S., Park, S. J., Seo, S. M., Yoo, Y. S., Jeong, H. W., and Jang, H. J. "High temperature oxidation resistance of Ni-(5~13)Co-(10~16)Cr-(5~9)W-5Al-(1~1.5)Ti-(3~6)Ta alloys." *Metals and Materials International*, Vol. 22, No. 5, (2016), 789–796. <https://doi.org/10.1007/s12540-016-6305-1>
 7. Duan, R., Jalowicka, A., Unocic, K., Pint, B. A., Huczowski, P., Chyrkin, A., Grüner, D., Pillai, R., and Quadakkers, W. J. "Predicting Oxidation-Limited Lifetime of Thin-Walled Components of NiCrW Alloy 230." *Oxidation of Metals*, Vol. 87, No. 1–2, (2017), 11–38. <https://doi.org/10.1007/s11085-016-9653-9>
 8. Sadeghimeresht, E., Reddy, L., Hussain, T., Huhtakangas, M., Markocsan, N., and Joshi, S. "Influence of KCl and HCl on high temperature corrosion of HVOF-sprayed NiCrAlY and NiCrMo coatings." *Materials and Design*, Vol. 148, (2018), 17–29. <https://doi.org/10.1016/j.matdes.2018.03.048>
 9. Yun, D. W., Seo, S. M., Jeong, H. W., and Yoo, Y. S. "Effect of refractory elements and Al on the high temperature oxidation of Ni-base superalloys and modelling of their oxidation resistance." *Journal of Alloys and Compounds*, Vol. 710, (2017), 8–19. <https://doi.org/10.1016/j.jallcom.2017.03.179>
 10. Gandomi, A. H., and Roke, D. A. "Assessment of artificial neural network and genetic programming as predictive tools." *Advances in Engineering Software*, Vol. 88, (2015), 63–72. <https://doi.org/10.1016/j.advengsoft.2015.05.007>
 11. Karahan, I. H., and Özdemir, R. "A comparison for grain size calculation of Cu-Zn alloys with genetic programming and neural networks." *Acta Physica Polonica A*, Vol. 128, No. 2, (2015), 427–431. <https://doi.org/10.12693/APhysPolA.128.B-427>
 12. Coşkun, M. İ., and Karahan, İ. H. "Modeling corrosion performance of the hydroxyapatite coated CoCrMo biomaterial alloys." *Journal of Alloys and Compounds*, Vol. 745, (2018), 840–848. <https://doi.org/10.1016/j.jallcom.2018.02.253>
 13. Ashtiani, H. R. R., and Shahsavari, P. "A comparative study on the phenomenological and artificial neural network models to predict hot deformation behavior of AlCuMgPb alloy." *Journal of Alloys and Compounds*, Vol. 687, (2016), 263–273. <https://doi.org/10.1016/j.jallcom.2016.04.300>
 14. Xu, D. S., Wang, H., Zhang, J. H., Bai, C. G., and Yang, R. "Titanium Alloys: From Properties Prediction to Performance Optimization." In *Handbook of Materials Modeling* (pp. 113–151), Springer International Publishing, 2020. https://doi.org/10.1007/978-3-319-44680-6_116
 15. Shakiba, M., Khayati, G. R., and Zeraati, M. "State-of-the-art predictive modeling of hydroxyapatite nanocrystallite size: a hybrid density functional theory and artificial neural networks." *Journal of Sol-Gel Science and Technology*, Vol. 92, No. 3, (2019), 641–651. <https://doi.org/10.1007/s10971-019-05113-0>
 16. Mahdavi Jafari, M., and Khayati, G. R. "Prediction of hydroxyapatite crystallite size prepared by sol–gel route: gene expression programming approach." *Journal of Sol-Gel Science and Technology*, Vol. 86, No. 1, (2018), 112–125. <https://doi.org/10.1007/s10971-018-4601-6>
 17. Jafari, M. M., Khayati, G. R., Hosseini, M., and Danesh-Manesh, H. "Modeling and Optimization of Roll-bonding Parameters for Bond Strength of Ti/Cu/Ti Clad Composites by Artificial Neural Networks and Genetic Algorithm." *International Journal of Engineering Transactions C: Aspects*, Vol. 30, No. 12, (2017), 1885–1893. <https://doi.org/10.5829/ije.2017.30.12c.10>
 18. Xu, C., Rangaiah, G. P., and Zhao, X. S. "Application of Artificial Neural Network and Genetic Programming in Modeling and Optimization of Ultraviolet Water Disinfection Reactors." *Chemical Engineering Communications*, Vol. 202, No. 11, (2015), 1415–1424. <https://doi.org/10.1080/00986445.2014.952813>
 19. Vakili, M., Khosrojerdi, S., Aghajannezhad, P., and Yahyaei, M. "A hybrid artificial neural network-genetic algorithm modeling approach for viscosity estimation of graphene nanoplatelets nanofluid using experimental data." *International Communications in Heat and Mass Transfer*, Vol. 82, (2017), 40–48. <https://doi.org/10.1016/j.icheatmasstransfer.2017.02.003>
 20. Raza, M. Q., and Khosravi, A. "A review on artificial intelligence based load demand forecasting techniques for smart grid and buildings." *Renewable and Sustainable Energy Reviews*, Vol. 50, (2015), 1352–1372. <https://doi.org/10.1016/j.rser.2015.04.065>
 21. khosrojerdi, S., Vakili, M., Yahyaei, M., and Kalhor, K. "Thermal conductivity modeling of graphene nanoplatelets/deionized water nanofluid by MLP neural network and theoretical modeling using experimental results." *International Communications in Heat and Mass Transfer*, Vol. 74, (2016), 11–17. <https://doi.org/10.1016/j.icheatmasstransfer.2016.03.010>
 22. Mahdavi, M., and Khayati, G. R. "Artificial Neural Network Based Prediction Hardness of Al2024-Multiwall Carbon Nanotube Composite Prepared by Mechanical Alloying." *International Journal of Engineering Transactions C: Aspects*, Vol. 29, No. 12, (2016), 1726–1733. <https://doi.org/10.5829/idosi.ije.2016.29.12c.11>
 23. Kalidass, S., and Mathavaraj Ravikumar, T. "Cutting Force Prediction in End Milling Process of AISI 304 Steel Using Solid Carbide Tools." *International Journal of Engineering, Transactions A: Basics*, Vol. 28, No. 7, (2015), 1074–1081. <https://doi.org/10.5829/idosi.ije.2015.28.07a.14>
 24. shafaei, A., and Khayati, G. R. "A predictive model on size of silver nanoparticles prepared by green synthesis method using hybrid artificial neural network-particle swarm optimization algorithm." *Measurement: Journal of the International Measurement Confederation*, Vol. 151, (2020), 107199. <https://doi.org/10.1016/j.measurement.2019.107199>
 25. da Silva, I. N., Hernane Spatti, D., Andrade Flauzino, R., Liboni, L. H. B., dos Reis Alves, S. F., da Silva, I. N., Hernane Spatti, D., Andrade Flauzino, R., Liboni, L. H. B., and dos Reis Alves, S. F. "Artificial Neural Network Architectures and Training Processes." In *Artificial Neural Networks* (pp. 21–28). Springer International Publishing, 2017. https://doi.org/10.1007/978-3-319-43162-8_2
 26. Maleki, E., and Kashyzadeh, K. R. "Effects of the hardened nickel coating on the fatigue behavior of CK45 steel: Experimental, finite element method, and artificial neural network modeling." *Iranian Journal of Materials Science and Engineering*, Vol. 14, No. 4, (2017), 81–99. <https://doi.org/10.22068/ijmse.14.4.81>
 27. Ansari, A., Heras, M., Nones, J., Mohammadpoor, M., and Torabi, F. "Predicting the performance of steam assisted gravity drainage (SAGD) method utilizing artificial neural network (ANN)." *Petroleum*, (2019). (In press) <https://doi.org/10.1016/j.petlm.2019.04.001>
 28. Gara, S., and Tsoumarev, O. "Optimization of cutting conditions in slotting of multidirectional CFRP laminate." *International Journal of Advanced Manufacturing Technology*, Vol. 95, No.

- 9–12, (2018), 3227–3242. <https://doi.org/10.1007/s00170-017-1451-2>
29. Gupta, I. K., Choubey, A., and Choubey, S. "Particle swarm optimization with selective multiple inertia weights." In 8th International Conference on Computing, Communications and Networking Technologies, (2017), 1-6. <https://doi.org/10.1109/ICCCNT.2017.8204132>
 30. Kumar, N., and Kumar Sharma, S. "Inertia weight controlled pso for task scheduling in cloud computing." In 2018 International Conference on Computing, Power and Communication Technologies, (2018), 155–160. <https://doi.org/10.1109/GUCON.2018.8674994>
 31. Nouri, M., Bekrar, A., Jemai, A., Niar, S., and Ammari, A. C. "An effective and distributed particle swarm optimization algorithm for flexible job-shop scheduling problem." *Journal of Intelligent Manufacturing*, Vol. 29, No. 3, (2018), 603–615. <https://doi.org/10.1007/s10845-015-1039-3>
 32. Ebrahimzade, H., Khayati, G. R., and Schaffie, M. "A novel predictive model for estimation of cobalt leaching from waste Li-ion batteries: Application of genetic programming for design." *Journal of Environmental Chemical Engineering*, Vol. 6, No. 4, (2018), 3999–4007. <https://doi.org/10.1016/j.jece.2018.05.045>
 33. Mansouri, I., Kisi, O., Sadeghian, P., Lee, C.-H., and Hu, J. "Prediction of Ultimate Strain and Strength of FRP-Confined Concrete Cylinders Using Soft Computing Methods." *Applied Sciences*, Vol. 7, No. 751, (2017), 1–14. <https://doi.org/10.3390/app7080751>
 34. Ferreira, C. "Gene Expression Programming in Problem Solving." In *Soft Computing and Industry* (pp. 635–653). Springer London, 2002. https://doi.org/10.1007/978-1-4471-0123-9_54
 35. Hoseinian, F. S., Faradonbeh, R. S., Abdollahzadeh, A., Rezai, B., and Soltani-Mohammadi, S. "Semi-autogenous mill power model development using gene expression programming." *Powder Technology*, Vol. 308, (2017), 61–69. <https://doi.org/10.1016/j.powtec.2016.11.045>
 36. Mansouri, I., Chacón, R., and Hu, J. W. "Improved predictive model to the cross-sectional resistance of CFT." *Journal of Mechanical Science and Technology*, Vol. 31, No. 8, (2017), 3887–3895. <https://doi.org/10.1007/s12206-017-0733-9>
 37. Mahdavi jafari, M., and Reza Khayati, G. "Adaptive neuro-fuzzy inference system and neural network in predicting the size of monodisperse silica and process optimization via simulated annealing algorithm." *Journal of Ultrafine Grained and Nanostructured Materials*, Vol. 51, No. 1, (2018), 43–52. <https://doi.org/10.22059/JUFGNSM.2018.01.06>
 38. Al-Mosawe, A., Kalfat, R., and Al-Mahaidi, R. "Strength of Cfrp-steel double strap joints under impact loads using genetic programming." *Composite Structures*, Vol. 160, (2017), 1205–1211. <https://doi.org/10.1016/j.compstruct.2016.11.016>
 39. Mansouri, I., Hu, J., and Kisi, O. "Novel Predictive Model of the Debonding Strength for Masonry Members Retrofitted with FRP." *Applied Sciences*, Vol. 6, No. 337, (2016), 1–13. <https://doi.org/10.3390/app6110337>
 40. Gholampour, A., Gandomi, A. H., and Ozbakkaloglu, T. "New formulations for mechanical properties of recycled aggregate concrete using gene expression programming." *Construction and Building Materials*, Vol. 130, (2017), 122–145. <https://doi.org/10.1016/j.conbuildmat.2016.10.114>
 41. Khandelwal, M., Armaghani, D. J., Faradonbeh, R. S., Ranjith, P. G., and Ghoraba, S. "A new model based on gene expression programming to estimate air flow in a single rock joint." *Environmental Earth Sciences*, Vol. 75, No. 9, (2016), 1–13. <https://doi.org/10.1007/s12665-016-5524-6>
 42. Bakhsheshi-Rad, H. R., Abdollahi, M., Hamzah, E., Ismail, A. F., and Bahmanpour, M. "Modelling corrosion rate of biodegradable magnesium-based alloys: The case study of Mg-Zn-RE-xCa (x = 0, 0.5, 1.5, 3 and 6 wt%) alloys." *Journal of Alloys and Compounds*, Vol. 687, (2016), 630–642. <https://doi.org/10.1016/j.jallcom.2016.06.149>
 43. Birks, N., Meier, G. H., and Pettit, F. S. *Introduction to the High Temperature Oxidation of Metals*. Cambridge University Press, 2006. Retrieved from <https://cds.cern.ch/record/1010949>
 44. Park, S.-J., Seo, S.-M., Yoo, Y.-S., Jeong, H.-W., and Jang, H. "Statistical Study of the Effects of the Composition on the Oxidation Resistance of Ni-Based Superalloys" *Journal of Nanomaterials*, Vol. 2015, (2015), 1–11. <https://doi.org/10.1155/2015/929546>

Persian Abstract

چکیده

در این مقاله سعی شده تا با در نظر گرفتن عناصر آلیاژی W، Cr و Mo، به عنوان متغیر، رفتار اکسیداسیون آلیاژهای پایه نیکل مدل‌سازی شود. برای نیل به این هدف از شبکه‌های عصبی مصنوعی بهینه‌سازی ذرات اصلاح شده (MPSO-ANN) و تکنیک‌های برنامه‌نویسی بیان ژن (GEP) استفاده شدند. برای ساخت مدل‌های (MPSO-ANN) و (GEP) از نتایج ۶۶ نمونه اکسیداسیون سیکلی در محدوده دمای ۴۰۰–۱۱۵۰ درجه سانتی‌گراد روی ۲۷ نمونه آلیاژ پایه نیکل با مقادیر مختلف W، Cr و Mo استفاده شد. درصد عناصر آلیاژی به عنوان متغیرهای ورودی و تغییر وزن در چرخه اکسیداسیون به عنوان خروجی مدل در نظر گرفته شدند. برای تحلیل عملکرد مدل‌های پیشنهادی، شاخص‌های مختلف آماری، مانند جذر میانگین خطای مربعات (RMSE) و ضریب همبستگی بین دو مجموعه داده (R^2) استفاده شد. داده‌های جمع‌آوری شده برای مدل‌سازی GEP به طور تصادفی به ۲۱ مجموعه داده آموزشی و ۶ مجموعه داده آزمایشی تقسیم گردید. نتایج تأیید کرد که امکان مدل‌سازی رفتار اکسیداسیون با استفاده از GEP با مقادیر $RMSE = 0.8822$ ، $R^2 = 0.981$ وجود دارد. با در نظر گرفتن مقاومت در برابر اکسیداسیون به عنوان معیار، مشخص شد که W، Cr و Mo مقاومت به اکسیداسیون آلیاژهای پایه نیکل را افزایش می‌دهد. همچنین، حضور کروم به عنوان عنصر آلیاژی، به‌ویژه در مقادیر بالاتر از ۲۲ درصد وزنی، تأثیر W و Mo را به مقدار زیادی کاهش می‌دهد. در حالی که حضور W و Mo در نمونه با محتوای کروم کمتر از ۲۰ درصد باعث بهبود قابل ملاحظه مقاومت به اکسیداسیون می‌شود.
